THE JOURNAL OF PHYSICAL CHEMISTRY B

Article

pubs.acs.org/JPCB

Predicting Elastic Properties of β-HMX from First-Principles Calculations

Qing Peng,*[,†] Rahul,[†] Guangyu Wang,[‡] Gui-Rong Liu,[‡] Stefan Grimme,[¶] and Suvranu De[†]

[†]Department of Mechanical, Aerospace and Nuclear Engineering, Rensselaer Polytechnic Institute, Troy, New York 12180, United States

[‡]School of Aerospace Systems, University of Cincinnati, Cincinnati, Ohio 45221, United States

[¶]Mulliken Center for Theoretical Chemistry, Institut für Physikalische und Theoretische Chemie, Rheinische Friedrich-Wilhelms Universität Bonn, Beringstrasse 4, 53115 Bonn, Germany

ABSTRACT: We investigate the performance of van der Waals (vdW) functions in predicting the elastic constants of β cyclotetramethylene tetranitramine (HMX) energetic molecular crystals using density functional theory (DFT) calculations. We confirm that the accuracy of the elastic constants is significantly improved using the vdW corrections with environment-dependent C_6 together with PBE and revised PBE exchange−correlation functionals. The elastic constants obtained using PBE-D3(0) calculations yield the most accurate mechanical response of β-HMX when compared with experimental stress−strain data. Our results suggest that PBE-D3 calculations are reliable in predicting the elastic constants of this material.

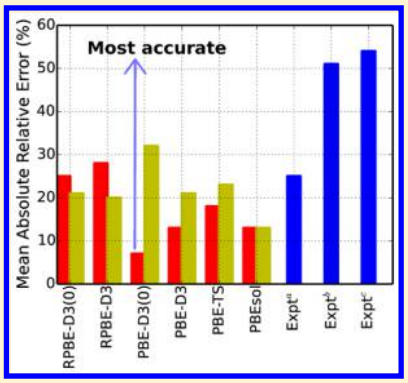

INTRODUCTION

There has been an increased interest in understanding and predicting the macroscopic response of energetic materials on the basis of mechanical properties, which are required in the formulation and parametrization of mesoscale continuum mechanical constitutive models.[1−8] The accurate prediction of the mechanical properties and crystallographic parameters are imperative to the development of physically based constitutive models that are necessary for continuum scale modeling of deformation mechanisms, which affect the sensitivity of energetic molecular crystals such as HMX.

HMX is an important secondary explosive that exists in three crystallographic polymorphs α, β, δ, and in hemihydrate γ form. The $P2_1/c$ monoclinic β-phase molecular crystal (Figure 1) is thermodynamically the most stable polymorph of HMX at room temperature.[9,10] β-HMX is a high-density energetic material with a high detonation velocity, which is most commonly used in military and industrial applications including polymer-bonded explosives and propellant formulations. Due to its importance, β-HMX has been the subject of extensive studies, both experimental (for example, refs 10−13) and theoretical, which include constitutive models,[1−8] molecular dynamics simulations,[14−17] and first-principles calculations.[18−20] The structures, mechanical properties, equations of state, and electronic properties of β-HMX under hydrostatic pressure were studied using a DFT-D2 method.[21] However, previous studies of the elastic constants were not satisfactory.

Elastic constants are among the most important physical characteristics of solid energetic materials as they provide a description of the mechanical behavior at the continuum level. Although first-principles calculations based on density functional theory (DFT) provide overall better predictive power than pure force-field models (for example, in ref 22), they fail in predicting lattice constants, volumes, and elastic constants of energetic materials with standard approximations, partially due to their poor descriptions of dispersion forces in molecular crystals.[21]

There are extensive studies to improve the modeling of dispersion, or van der Waals (vdW) interactions.[23] Although there are significant improvements referring to standard DFT calculations, previous modeling efforts[18,24,25] with vdW corrections in DFT-D1[26] and DFT-D2[27] methods still show considerable errors in densities compared to experiments. Recently, more accurate methods that account for vdW interactions, such as the D3 correction method of Grimme et al. (denoted as DFT-D3(0) hereafter),[28,29] modified with Becke-Johnson damping (denoted as DFT-D3),[30] and Tkatchenko-Scheffler (denoted as DFT-TS) method[31] and its self-consistent screening derivatives (denoted as DFT-TS-SCS)[32] were invented. The DFT-D3(0) method is a consistent and accurate ab initio parametrization of density functional dispersion corrections, developed for 94 elements from H to Pu. Unlike the DFT-D2 method, the dispersion coefficients in DFT-D3(0) are geometry dependent. DFT-D3 uses a damping function different from the one in DFT-D3(0). In the DFT-TS method, the dispersion coefficients and damping function are

Received: January 5, 2015
Revised: April 7, 2015

DOI: 10.1021/acs.jpcb.5b00083
J. Phys. Chem. B XXXX, XXX, XXX−XXX

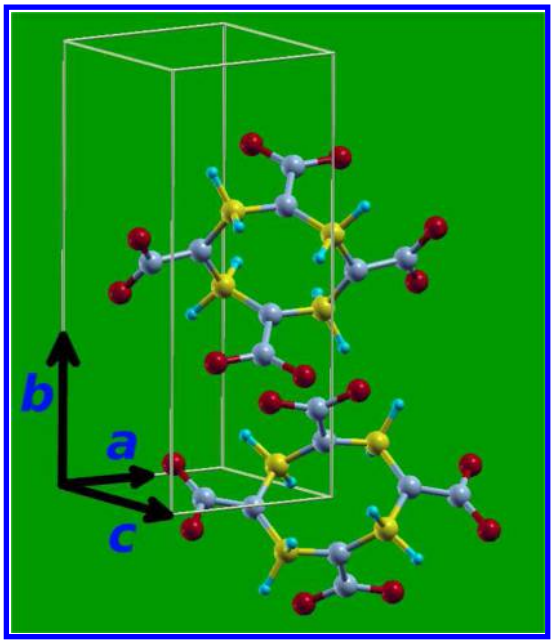

Figure 1. Geometry of β-HMX. The primitive unit cell of β-HMX containing two HMX molecules with centro-symmetric structure. The four carbon atoms (yellow) and four nitrogen atoms (gray) form a ring−chain.

charge-density dependent compared to DFT-D2. As a result, it can take into account variations in vdW contributions of atoms due to their local chemical environment. Its derivative, the DFT-TS-SCS method, accounts for electrodynamic response effects. The DFT-D1 and DFT-D2 methods are classified as the first rung of Jacob's Ladder for DFT-based dispersion correction schemes.[23] The DFT-D3, DFT-D3(0), DFT-TS, and DFT-TS-SCS methods belong to the second rung that utilizes environment dependent C_6 corrections. Long-range density functionals like DFT-DF and DFT-DF2 methods sit in the third rung,[23] of which overall accuracy is expected to increase, as well as computational demand. The application of these newly developed methods in studying the structural properties and elastic constants of β-HMX needs further investigation. In this paper, we focus on the DFT-D3(0), DFT-D3, and DFT-TS methods. In addition, we limit our study on HMX because to the best of the authors' knowledge, there is only one experimental stress−strain data[33] of energetic materials (HMX) available for validation.

METHODOLOGY

First-Principles Calculations. We consider a conventional unit cell containing two HMX molecules (56 atoms in total) with periodic boundary conditions. The total energies of the system, forces on each atom, stresses, and stress−strain relationships of β-HMX under the desired deformation configurations are characterized via first-principles calculations based on density-functional theory (DFT). DFT calculations were carried out with the Vienna Ab-initio Simulation Package (VASP)[34,35] which is based on Kohn−Sham Density Functional Theory (KS-DFT)[36,37] with the generalized gradient approximation as parametrized by Perdew, Burke, and Ernzerhof (PBE) for exchange−correlation functionals.[38] We also examine two other exchange−correlation functionals: revised Perdew−Burke−Ernzerhof (RPBE)[39] and Perdew−Burke−Ernzerhof revised for solids (PBEsol).[40]

The electrons explicitly included in the calculations are the $1s^1$ for hydrogen atoms, $2s^22p^4$ for carbon atoms, $2s^22p^5$ for nitrogen atoms, and $2s^22p^6$ for oxygen atoms. The core electrons are replaced by the projector augmented wave (PAW) and pseudopotential approach.[41,42] The kinetic-energy cutoff for the plane-wave basis was selected to be 800 eV in this study. The calculations are performed at zero temperature.

The criterion to stop the relaxation of the electronic degrees of freedom is set by the total energy change to be smaller than 0.000001 eV. The optimized atomic geometry was achieved through minimizing Hellmann−Feynman forces acting on each atom until the maximum forces on the ions were smaller than 0.001 eV/Å. The atomic structures of all the deformed and undeformed configurations were obtained by fully relaxing unit cells. The simulation invokes periodic boundary conditions in the x, y, and z directions. The irreducible Brillouin Zone was sampled with a $5 \times 3 \times 4$ Gamma-centered k-mesh. The initial charge densities were taken as a superposition of atomic charge densities.

van der Waals Corrections. In the DFT-D2 method,[27] the van der Waals interactions are described using a pairwise force field. Such a semiempirical dispersion potential is then added to the conventional Kohn−Sham DFT energy as $E_{\mathrm{DFT-D2}} = E_{\mathrm{DFT}}+E_{\mathrm{disp}}$ and

$$E_{\mathrm{disp}}^{D2} = -\frac{1}{2}\sum_{i=1}^{N}\sum_{j=1}^{N}\sum_{L}{}'\frac{C_{6,ij}}{r_{ij,L}^{6}}f_{d,6}(r_{ij,L}) \tag{1}$$

where N is the number of atoms. The summations go over all atoms and all translations of the unit cell $L = (l_1,l_2,l_3)$. The prime indicates that for $L = 0$, $i \neq j$. $C_{6,ij} = (C_{6,ii}C_{6,jj})^{1/2}$ stands for the dispersion coefficient for the atom pair ij. $r_{ij,L}$ is the distance between atom i in the reference cell $L = 0$ and atom j in the cell L. $f(r)$ is a damping function whose role is to scale the force field such as to minimize contributions from interactions within typical bonding distances r. Because the van der Waals interactions decay quickly in the power of -6, the contributions outside a certain suitably chosen cutoff radius are negligible. The cutoff radius for pair interactions in this study is set to 30.0 Å. Here a Fermi-type damping function is used as

$$f_{d,6}(r_{ij}) = \frac{s_6}{1 + \mathrm{e}^{-d\left(\frac{r_{ij}}{s_r R_{0ij}}-1\right)}} \tag{2}$$

where S_6 is the global scaling parameter, $R_{0ij} = R_{0i}+R_{0j}$. The global scaling factor $S_6 = 0.75$ is used for PBE exchange−correlation functions. s_r is fixed at 1.00. The damping parameter $d = 20.0$ is used.

Compared to the DFT-D2 method, the DFT-D1 method[26] has a few shortcomings: (1) It has parameters available only for elements H and C through Ne. (2) There are systematic errors for calculations of molecules containing third-row elements. (3) It leads to inconsistencies for thermochemistry due to the double-counting problem.[27] In addition to overcoming these shortcomings, DFT-D2 generalized the dispersion correction and improved the accuracy.

In the DFT-D3(0) method,[28] there is one more term in the van der Waals interaction compared to the previous DFT-D2 method, as

$$E_{\mathrm{disp}}^{D3} = E_{\mathrm{disp}}^{D2} - \frac{1}{2}\sum_{i=1}^{N}\sum_{j=1}^{N}\sum_{L}{}'\frac{C_{8,ij}}{r_{ij,L}^{8}}f_{d,8}(r_{ij,L}) \tag{3}$$

DOI: 10.1021/acs.jpcb.5b00083
J. Phys. Chem. B XXXX, XXX, XXX−XXX

Table 1. Geometry Lattice Constants *a*,*b*,*c*, Lattice Angle β, Volume of the Unit Cell *V*, and Density ρ Predicted from First-Principles Calculations, Compared with Experiments and Previous Calculations[a]

	a (Å)	*b* (Å)	*c* (Å)	β	*V* (Å^3)	ρ (10^3kg/m^3)
expt[b]	6.54	11.05	8.70	124.30	519.39	1.894
expt[c]	6.537	11.054	8.7018	124.443	518.558	1.897
expt[d]	6.495(±0.014)	10.952(±0.010)	8.693(±0.024)	124.53(±0.20)	509.44	1.931
expt[e]	6.5255(±0.0010)	11.0369(±0.0018)	7.3640(±0.0012)	102.670(±0.010)	517.45(±0.14)	1.901
theory[f]	6.70(+2.45%)	11.35(+2.71%)	8.91(+2.41%)	124.13(−0.14%)	560.86(+7.98%)	1.754(−7.39%)
PBE[g]	6.673(+2.03%)	11.312(+2.37%)	8.894(+2.23%)	124.395(+0.08%)	553.99(+6.66%	1.775(−6.23%)
PBE-D2[g]	6.542(+0.03%)	10.842(−1.88%)	8.745(+0.52%)	124.41(+0.09%)	511.73(−1.47%)	1.923(+1.53%)
PBE-D3(0)	6.541(+0.02%)	10.894(−1.41%)	8.748(+0.55%)	124.38(+0.06%)	514.488(−0.94%)	1.912(+0.95%)
PBE-D3	6.550(0.15%)	10.899(−1.37%)	8.763(0.72%)	124.416(+22%)	516.062(−0.64%)	1.906(+0.64%)
PBE-TS	6.530(−0.15%)	10.985(−0.59%)	8.770(+0.80%)	124.572(+0.22%)	517.992(−0.27%)	1.899(+0.27%)
RPBE-D3(0)	6.580(+0.61%)	11.061(−0.1%)	8.762(+0.71%)	124.357(+0.05%)	526.501(−1.37%)	1.868(−1.35%)
RPBE-D3	6.616(+1.16%)	11.044(−0.05%)	8.785(+0.98%)	124.174(−0.1%)	531.093(−2.25%)	1.852(−2.20%)
PBEsol	6.603(+0.96%)	10.928(−1.10%)	8.709(+0.10%)	124.002(−0.24%)	520.949(0.30%)	1.888(−0.30%)

[a]The numbers in parentheses are differences in percentage referring to the experiment. [b]ref 11. [c]ref 45. [d]ref 10. [e]303 K space group $P2_1/n$ in ref 46. [f]DFT study using PAW−PBE(GGA) in ref 18. [g]ref 21.

In addition, the dispersion coefficients $C_{6,ij}$ are geometry-dependent, so that they are adjustable according to the local geometry around atoms *i* and *j* through their coordination number. The damping function is

$$f_{d,n}(r_{ij}) = \frac{s_n}{1 + 6(r_{ij}/(s_{R,n}R_{0ij}))^{-\alpha_n}} \tag{4}$$

where *n* is the order (6 or 8), $R_{0ij} = (C_{8,ij}/C_{6,ij})^{1/2}$, the parameters $\alpha_6 = 14$, $\alpha_8 = 16$, $s_{R,8} = 1$. The values of s_6, s_8, and $R_{R,6}$ are adjustable with respect to the choice of the exchange−correlation functional. A cutoff radius of 50.2 Å is used for pair interactions in eq 3. For calculating the coordination number, a cutoff radius of 20.0 Å is used.

In the DFT-D3 method that is currently the recommended default for general use, the damping approach of Becke and Johnson with the same dispersion coefficients and three empirical parameters per functional is used (see ref 30 for details).

In the DFT-TS method,[31] the same expression as the DFT-D2 method (eq 1) for the van der Waals interactions is used. However, the dispersion coefficients and damping function in DFT-TS are charge-density-dependent, as opposed to the fixed values in DFT-D2. Note that these variables are *geometry*-dependent in the DFT-D3(0) method with the exclusion of an additional term. Because the dispersion coefficients and damping function are adjustable according to the environments, DFT-TS and DFT-D3(0), as well as DFT-D3, can take into account variations in van der Waals contributions of atoms due to their local status and configurations, and therefore be more powerful in modeling molecular crystals.

Continuum Modeling. In the theory of linear elasticity, the second order strain tensor and the corresponding work conjugate stress tensor is related through the fourth order elasticity tensor and is often referred to as the generalized Hooke's law, which incorporates fully anisotropic material responses.[43] The stress−strain response is then obtained by solving governing equations of elastostatics in conjugation with the constitutive relation using the finite element method.[44] For the implementation details and solution methodology, we refer to our recent publications.[2−4] Here is a brief introduction for the continuum modeling.

For a macroscopically homogeneous body that occupies a bound domain $\Omega \subset \mathbb{R}^d$; $d \in \{1,2,3\}$ with boundary $\Gamma = \Gamma_t \cup \Gamma_u$; $\Gamma_t \cap \Gamma_u = \phi$, where Γ_u and Γ_t are the Dirichlet and Neumann boundaries, respectively, in Euclidean space, the governing equations of elastostatics are given by the balance of linear and angular momenta

$$\begin{cases} \text{div}\,\sigma + \rho\mathbf{b} = 0, \text{ in } \Omega \\ \sigma^T = \sigma \end{cases} \tag{5}$$

with boundary conditions

$$\mathbf{u} = \bar{\mathbf{u}}, \text{ on } \Gamma_u \tag{6}$$

$$\sigma\hat{\mathbf{n}} = \bar{\mathbf{t}}, \text{ on } \Gamma_t \tag{7}$$

along with the strain−displacement relationship

$$\epsilon = \frac{1}{2}(\nabla\mathbf{u} + \nabla\mathbf{u}^T) \tag{8}$$

where σ denotes the second order Cauchy stress tensor, $\rho\mathbf{b}$ is the body force per unit volume, $\bar{\mathbf{t}}$ is the surface traction on Γ_t, $\bar{\mathbf{u}}$ is the prescribed displacement on Γ_u, $\hat{\mathbf{n}}$ is the unit outward normal to Γ_t, ϵ is the second order strain tensor and the corresponding work conjugate stress tensor is σ, and div(.) is the divergence operator.

The generalized Hooke's law incorporates the fully anisotropic material response as

$$\sigma = \mathbf{C}\colon \epsilon \tag{9}$$

where $\mathbf{C}$ is a fourth order elasticity tensor, which is dependent on the crystal orientation. It can be expressed as

$$\mathbf{C} = \mathbf{R}\colon \mathbf{R}\colon \mathbf{C}'\colon \mathbf{R}^T\colon \mathbf{R}^T \tag{10}$$

where $\mathbf{C}'$ is the elastic tensor with respect to the base vector of the crystal, and $\mathbf{R}$ is the orientation matrix that rotates the current base vector to the global sample coordinate system.

RESULTS AND ANALYSIS

Atomic Structure and Geometry. First, we fix the geometry of the primitive unit cell of the monoclinic crystal of β-HMX to the experimental value,[11] which is $a = 6.54$ Å, $b = 11.05$ Å, $c = 8.70$ Å, and the angle is 124.30° (*a*,*b*,*c* are shown in Figure 1). The atoms are then relaxed to the configuration of the energy minimum. We also examined the case where the geometry of the primitive unit cell is optimized by fully relaxing all of the atoms and lattice constants. The optimized lattice

DOI: 10.1021/acs.jpcb.5b00083
J. Phys. Chem. B XXXX, XXX, XXX−XXX

Table 2. Thirteen Non-Zero Elastic Constants C_{ij}, Bulk Moduli B, Shear Moduli G, Poisson's Ratios ν, and Cauchy Pressures C_P of β-HMX That Are Predicted Using DFT Calculations, Compared with Experiments and Previous Calculations[a]

	C_{11}	C_{12}	C_{13}	C_{15}	C_{22}	C_{23}	C_{25}	C_{33}	C_{35}	C_{44}	C_{46}	C_{55}	C_{66}	B	G	ν	C_P
expt[b]	20.58	9.65	9.75	−0.61	19.69	12.93	4.89	18.24	1.57	9.92	4.42	7.69	10.67	13.69	7.40	0.271	−0.27
expt[c]	18.41	6.37	10.50	−1.10	14.41	6.42	0.83	12.44	1.08	4.77	2.75	4.77	4.46	10.20	4.26	0.317	1.6
expt[d]	20.8	4.8	12.5	−0.5	26.9	5.8	−1.9	18.5	1.9	4.2	2.9	6.1	2.5	12.49	5.43	0.310	0.6
PBE[e]	75.1	18.6	1.4	−23.4	28.9	24.6	1.0	44.5	−14.2	23.4	−8.0	18.7	28.7	26.41	21.09	0.185	−4.8
PBE-D2[e]	29.3	10.6	13.8	−2.1	25.0	16.6	6.2	27.5	1.1	13.6	6.8	12.8	13.9	18.20	10.78	0.253	−3.0
PBE-D3(0)[§]	24.1	10.0	9.4	−1.1	23.0	14.0	4.4	22.1	3.8	11.7	7.0	7.9	8.3	15.1	8.0	0.275	−1.7
PBE-D3[§]	19.8	7.2	7.1	−1.3	20.5	11.0	5.1	18.2	4.0	12.9	6.0	8.5	10.9	12.09	8.69	0.210	−5.8
PBE-TS[§]	22.9	7.1	9.3	−3.0	20.8	12.2	4.9	21.2	2.9	12.6	5.8	10.1	13.3	13.58	9.61	0.214	−5.4
PBE-D3(0)*	26.1	10.5	11.0	−1.2	24.8	15.6	5.4	27.9	1.8	13.3	5.2	10.5	14.0	17.0	10.3	0.247	−2.8
PBE-D3*	24.0	10.4	10.9	−0.9	23.0	14.1	4.6	25.2	1.0	11.4	5.7	10.4	12.6	15.9	9.3	0.255	−1.0
PBE- TS*	27.6	10.3	11.8	−3.1	23.4	14.1	5.0	24.1	0.9	12.1	5.1	10.8	13.1	16.4	9.8	0.251	−1.8
RPBE-D3(0)[§]	26.6	9.4	11.3	−1.7	23.8	13.7	6.1	25.6	0.3	13.3	6.2	11.6	12.5	16.1	10.3	0.237	−3.9
RPBE-D3(0)*	25.0	8.7	10.2	−2.0	22.2	12.7	5.3	24.0	0.1	12.0	5.6	11.2	12.5	14.9	9.8	0.231	−3.3
RPBE-D3[§]	26.9	10.2	10.9	−2.9	21.4	13.8	4.5	21.6	−0.1	11.8	5.5	11.0	11.6	15.5	9.2	0.252	−1.6
RPBE-D3*	21.0	8.7	8.0	−0.4	20.1	10.9	4.7	20.3	0.8	10.8	4.5	9.1	11.6	13.0	8.5	0.230	−2.0
PBEsol[§]	19.7	9.0	8.2	−0.3	17.7	7.7	3.8	18.2	0.2	9.2	4.1	8.0	10.0	11.7	7.5	0.237	−0.2
PBEsol*	17.9	7.2	5.1	1.2	17.0	6.9	4.3	16.9	1.5	8.3	4.0	6.7	9.3	10.0	6.9	0.220	−1.1

[a]Units are in GPa with the exception of Poisson's ratio. [b]ref 48. [c]ref 12. [d]ref 13. [e]ref 21. [§]Fix the geometry (lattice constants) of the unit cells as experimental value, ref 48. [*]The lattice constants of the unit cells are optimized.

DOI: 10.1021/acs.jpcb.5b00083
J. Phys. Chem. B XXXX, XXX, XXX−XXX

constants using PBE-D3(0), PBE-D3, PBE-TS, RPBE-D3(0), RPBE-D3, and PBEsol are summarized in Table 1, along with the volumes and the densities. The difference referring to the experimental value[11] in percentages are shown in parentheses next to their respective values. Our optimized crystal structure has a space group of $P2_1/c$.

The four experiments listed in Table 1 are in chronological order. Choi and Boutin studied the crystal structure using neutron diffraction,[11] which is one of the early experimental measurements and is widely accepted. Thus, we take it as a "standard" experimental value in this study. Herrmann et al.[45] measured the crystal structures under various temperatures using X-ray diffraction. Yoo and Cynn examined the crystal structures under pressure using diamond-anvil cell, angle-resolved synchrotron X-ray diffraction, and micro-Raman spectroscopy.[10] Recently, Deschamps et al. studied the thermal expansion of β-HMX using X-ray diffraction and the crystal structure data was reported to be in space group $P2_1/n$.[46] The standard deviations of the experimental measurements[10,46] are also listed in Table 1. The standard DFT calculations (denoted as PBE hereafter) without van der Waals corrections agree well with the previous theoretical prediction.[18] It shows that standard DFT calculations give poor predictions. For example, the volume of the unit cell is 6.7% higher than the experimental value. The density of β-HMX from DFT-D2 calculations (denoted as PBE-D2 hereafter) is more accurate, with a difference of −1.47% compared to the experimental value.[11] The accuracy is within the variation of experimental values, which is 1.95% difference between Yoo's and Choi's measurements. This is a significant improvement over standard DFT calculations without van der Waals corrections as reported in our previous work.[21] In this study, we found that PBE-D3(0), PBE-D3, PBE-TS, and PBEsol further increase the accuracy to be within 1%. However, RPBE-D3(0) and RPBE-D3 do not yield such an increment in accuracy.

Elastic Properties. The elastic constants are the second derivatives of the total energy with regard to strain. Our results of all 13 elastic constants, in standard Voigt notation,[47] are listed in Table 2, and are compared with experiments and theoretical predictions. The one nonstandard cell commonly used is $P2_1/n$ which is derived from $P2_1/c$. The lattice vectors $\mathbf{a}_0$, $\mathbf{b}_0$, and $\mathbf{c}_0$ in space group $P2_1/n$ can be transformed to space group $P2_1/c$ as $\mathbf{a} = -\mathbf{a}_0$, $\mathbf{b} = -\mathbf{b}_0$, and $\mathbf{c} = \mathbf{a}_0+\mathbf{b}_0$.

For a valid comparison, the Cartesian system to which the elastic constants are referenced must be the same for all these data sets. We used the reference system of the x and y axes parallel to the a- and b-crystallographic axes, respectively, which is the same as Sewell et al.[14,49] and Stevens and Eckhardt.[12] Zaug's results (expt^c in Table 1) were transformed to this Cartesian system by Sewell. Note that the experimental studies prefer using the $P2_1/n$ space group to the standard $P2_1/c$ space group. The elastic constants in these two space groups are identical except that $C^c_{15} = -C^n_{15}$, $C^c_{25} = -C^n_{25}$, $C^c_{35} = -C^n_{35}$, and $C^c_{46} = -C^n_{46}$, where super indices c and n refer to space group $P2_1/c$ and $P2_1/n$, respectively. Our data in Table Table 1 are transformed from the form of C^c_{ij} into the form of C^n_{ij}.

The combination of PBEsol with vdW functions gives a large error in predicting the density (larger than 6%) due to double counting of the nonlocal interactions. Therefore, it has not been used to predict the elastic constants as they are expected to have large errors. Overall, although the predictions from standard DFT studies differ greatly from experiments, the elastic constants obtained using PBE-D3(0), PBE-D3, and PBE-TS methods agree much better with the experiments, which is a significant improvement over DFT-D2 calculations.[21] This is expected as the D3(0), D3, and TS vdW corrections belong to the second rung of the Jacob's Ladder.[23] The results from RPBE-D3(0) and RPBE-D3 calculations assist our findings. The results from DFT-PBEsol calculations without vdW corrections also agree well with the experiments.

The bulk modulus B measures the resistance to hydrostatic compression and it can be calculated using the Voigt notation from the elastic constants as

$$B = \frac{1}{9}\sum_{i,j}^{3} C_{ij} \tag{11}$$

For example, taking our PBE results corresponding to the PBE-D3(0), PBE-D3, and PBE-TS methods, the bulk moduli are 15.1, 12.1, and 13.6 GPa, respectively. These values are comparable to an average value of 12.1 GPa for the three sets of experimental data. The accuracy of the predicted bulk modulus of β-HMX has been significantly improved using these three methods in comparison with the previous results that are obtained using DFT and DFT-D2 calculations.[21] It is well-known that the theoretical elastic constants are often stiffer compared to those of experiments. This overestimation is attributed to two factors: the use of the rigid-body approximation for flexible molecules, and the neglect of the anharmonic softening of the lattice at finite temperatures. Our DFT studies are performed at zero temperature where the thermodynamics as well as the anharmonic softening are excluded. This is reflected in the larger value of our predicted bulk modulus.

The shear modulus measures the resistance in shearing, which can be calculated using the Voigt notation from elastic constants as

$$G = \frac{1}{15}(C_{11} + C_{22} + C_{33} - C_{12} - C_{23} - C_{13}) + \frac{1}{5}(C_{44} + C_{55} + C_{66}) \tag{12}$$

The shear deformations have been proposed to be a critical component in the initiation of detonation. Therefore, a precise determination of the shear modulus is necessary for substantiating possible detonation mechanisms. Our calculations predict a shear modulus of 8.0, 8.69, and 9.61 GPa corresponding to the PBE-D3(0), PBE-D3, and PBE-TS methods, respectively. These values are larger than the average value 5.7 GPa of the experimental values. This is partially attributed to the preclusion of the anharmonic softening of the lattice with temperature. In comparison with the previous results obtained using DFT and DFT-D2 methods, the shear modulus predicted using PBE-D3(0), PBE-D3, and PBE-TS calculations is much more accurate.

The Poisson's ratio measures the shape change under mechanical loading, offering the fundamental metric by which to compare the performance of any material when strained elastically.[50] For an isotropic material, the Poisson ratio ν is related with bulk moduli and shear moduli as

$$\nu = \frac{3B - 2G}{2(3B + G)} \tag{13}$$

The calculated values of the Poisson's ratio corresponding to the PBE-D3(0), PBE-D3, and PBE-TS methods are 0.275,

DOI: 10.1021/acs.jpcb.5b00083
J. Phys. Chem. B XXXX, XXX, XXX−XXX

0.210, and 0.214, respectively, which are smaller than the average (0.299) of the experimental values.

The Cauchy pressure $C_P = C_{12}-C_{44}$ can be used to evaluate the ductibility of a material.[51] A positive value of C_P indicates that the material is ductile, whereas a negative value implies a brittle material. The results of ductibility from both experiments and molecular dynamics studies are controversial. For example, experiments[48] indicate β-HMX is brittle, however, another two[12,13] imply that the β-HMX is ductile. The average C_P of the experiments is 0.64. Our DFT-D3(0), DFT-D3, and DFT-TS studies indicate that the β-HMX is brittle. The DFT-D3 and DFT-TS calculations give much larger values of C_P than experiment. There are two possible reasons for this: First, the simulation boxes in the DFT-D3(0), DFT-D3, and DFT-TS modeling are small, which excludes the long wavelength phonon modes that contribute to the ductility. Second, the zero temperature applied in our models precludes thermodynamic effects, which is essential for the ductility. As a result, the ductibility of our models appears to be much smaller than experimental values.

The diagonal elements C_{ii} describe the crystal stiffness under uniaxial compression (i = 1,2,3) and shear (i = 4,5,6), whereas the off-diagonal elements $C_{i\neq j}$ represent the crystal stiffness under biaxial compression ($i \neq j$ = 1,2,3) and distortion ($i \neq j$ = 4,5,6). Our results show that there is a remarkable anisotropy in the diagonal elements of the elasticity tensor. Furthermore, they indicate that the β-HMX is anisotropic upon compression and has a good stability to shear deformation perpendicular to the c-axis.

Here, C_{22} is relevant to the "doorway mode" anharmonic coupling model, which is an important feature for detonation of secondary explosives.[52] Experimental and theoretical vibration analysis illustrates the presence of low-energy modes that have the necessary symmetry for such anharmonic coupling. The experimental value of C_{22} varies from 14.41 to 26.9 GPa, with an average of 19.63 GPa. Our predicted value of C_{22} is 23.0, 20.5, and 20.8 GPa from DFT-D3(0), DFT-D3, and DFT-TS studies, respectively, which agrees well with the experiments. In comparison with the previous results predicted by DFT and DFT-D2 methods, the C_{22} values predicted using PBE-D3(0), PBE-D3, and PBE-TS methods are much more accurate.

Stress–Strain Relationship. In addition to the comparison with experimental values of elastic constants, we validate these elastic constants by comparing the interpolated mechanical behaviors with the experimentally measured quasi-static compressive stress versus strain response of single crystals of β-HMX.[33] A finite element computational model is developed to simulate the displacement controlled uniaxial compression test on a 5 × 5 × 3 mm^3 sample of β-HMX molecular single crystal. The faces of the rectangular block initially normal to the compressive axis remain normal to that axis. The sample domain is discretized using 9375 trilinear hexahedral finite elements with eight Gauss points per element. The stress–strain curves of β-HMX are obtained using the anisotropic elasticity tensor C_{ij}.

The uniaxial compressive strains are applied on a β-HMX single crystal on its (110) plane and along the [001] direction. We only plot the stress–strain responses within the elastic limits. In Figure 2, we compare the simulation results with the experimental stress–strain data[33] for these two loading conditions. While the stress–strain response corresponding to DFT-vdW calculations are in close agreement with the experimental stress–strain data for loading along the [001] direction (Figure 2b), DFT-TS and DFT-D3 are most accurate for loading on the (110) plane (Figure 2a). Therefore, we may conclude that the elastic constants obtained using DFT-TS and DFT-D3 calculations yield the most accurate prediction of the mechanical response compared with others for this material. It is worth noting that the predicted behavior using the standard DFT calculations differs greatly with the experimental stress–strain curve, and therefore, we have not plotted it here.

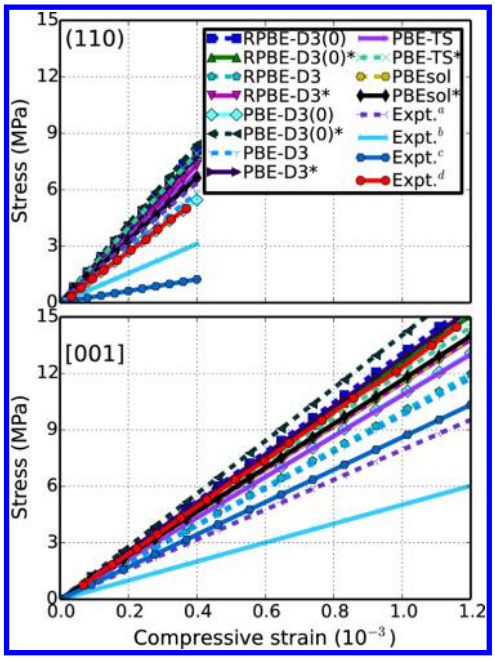

Figure 2. Mechanical response of β-HMX. Comparison of the stress–strain response of β-HMX at the continuum level corresponding to the elastic constants listed in Table 2, with experimental observations[33] (denoted as Expt^e). The three sets of elastic constants measured from experiments[12,13,48] are denoted as Expt^a-Expt^c. The rest are from theoretical calculations, where those with ∗ use the optimized unit cells. The uniaxial compressive strain is applied (a) on the (110) plane, and (b) along the [001] direction. Note that the ranges of stresses are up to elastic limits.

We use the Mean Absolute Relative Error (MARE) to measure the quality of the calculated elastic constants. The experimental stress–strain data[33] are set as the reference. The MAREs of the data shown in Figure 2 are plotted in Figure 3. A smaller value of MARE means a higher accuracy. Here we have four observations. First of all, our DFT calculations have smaller MAREs than some experiments, implying that our results agree well with experiments. Second, we compared the results using optimized cells with those using experimental cells. We observe that the DFT calculations with the RPBE exchange–correlation functional using optimized cells have higher accuracy than those using experimental cells, as opposed to those from DFT calculations with the PBE exchange–correlation functional. The results of DFT-PBEsol calculations have the same accuracy for these two conditions. We notice that the accuracy using the optimized cells is less sensitive to the choice of van der Waals functionals than those using experimental cells, and the accuracy is around 20%. Thus, it might be more reasonable to optimize the cells before the calculations of the elastic constants. Third, we study the differences applying different van der Waals corrections using the same (experimental) unit cell. The order of the accuracy from these three tested van der Waals formula (D3(0), D3, and

DOI: 10.1021/acs.jpcb.5b00083
J. Phys. Chem. B XXXX, XXX, XXX–XXX

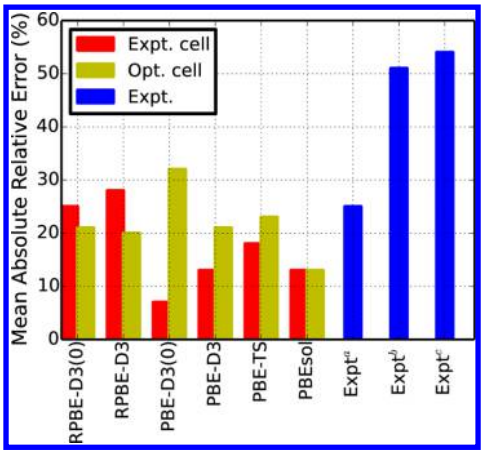

Figure 3. MARE of the stress−strain data. The Mean Absolute Relative Errors of the stress−strain data interpolated from the elastic constants are referred to the raw experimental stress−strain data.[33] The red bars are for those elastic constants that are calculated using fixed experimental unit cells. The yellow bars are for those calculated using optimized unit cells. The blue bars are for the experimentally measured elastic constants as listed in Table 1.

TS), is D3(0) > D3 > TS. But for optimized unit cells, D3 performs better than D3(0). Fourth, we examine the difference from the exchange−correlation functionals. The two exchange−correlation functionals of PBE and RPBE with vdW corrections and the PBEsol alone can predict the elastic constants with an accuracy smaller than 30% in MARE, which is within the accuracy of experimental measurements. The PBE-D3(0) gives the most accurate prediction of elastic constants among the tested cases. However, it is unrealistic to draw a decisive conclusion that PBE-D3(0) has better performance than other combinations of exchange−correlation functionals and van der Waals corrections. Considering the computing complexity, the PBEsol alone (without vdW corrections) might still be the best choice for this molecular crystal.

CONCLUSIONS

In summary, we have studied the structural and mechanical properties of β-HMX using DFT calculations with several combinations of exchange−correlation functionals and vdW functions. Two conditions were examined: one with the fixed experimental unit cells and the other with optimized unit cells starting from experimental values before the calculations of the elastic constants. The accuracy of the elastic constants of β-HMX is significantly improved using van der Waals corrections compared to the standard DFT calculations as well as DFT-D2. The PBE and revised PBE exchange−correlation functionals combined with the D3(0), D3, and TS flavors of vdW functions can predict the elastic constants within a 30% accuracy when compared with experimental measurements. However, PBEsol alone (without van der Waals corrections) can achieve the same goal. Among the 14 examined cases, the DFT-PBE-D3(0) calculation with the experimental unit cell has the highest accuracy, about 7%, when compared with the experimental stress−strain data. Our results suggest that the van der Waals interactions are critically important in modeling mechanical properties and DFT-PBE-D3 is reliable in predicting the elastic constants of this molecular crystal. Therefore, we call for great attention to the theoretical community when using density functionals to investigate molecular crystals and energetic materials.

AUTHOR INFORMATION

Corresponding Author

*E-mail: qpeng.org@gmail.com.

Notes

The authors declare no competing financial interest.

ACKNOWLEDGMENTS

We thank Bernd Hartke and Shengbai Zhang for helpful discussions. The authors would like to acknowledge the generous financial support from the Defense Threat Reduction Agency (DTRA) Grant No. HDTRA1-13-1-0025 and the Office of Naval Research grants ONR Award No. N00014-08-1-0462 and No. N00014-12-1-0527. Computational resources were provided by Rensselaer Polytechnic Institute through AMOS, the IBM Blue Gene/Q system at the Center for Computational Innovations.

REFERENCES

(1) Clayton, J. D.; Becker, R. Elastic-plastic behavior of cyclotrimethylene trinitramine single crystals under spherical indentation: Modeling and simulation. *J. Appl. Phys.* **2012**, *111*, 063512.

(2) De, S.; Zamiri, A. R. Rahul, A fully anisotropic single crystal model for high strain rate loading conditions with an application to α-RDX. *J. Mech. Phys. Solids* **2014**, *64*, 287−301.

(3) Zamiri, A. R.; De, S. Modeling the anisotropic deformation response of β-HMX molecular crystals. *Propellants, Explosives, Pyrotechnics* **2011**, *36*, 247−251.

(4) Zamiri, A. R.; De, S. Deformation distribution maps of β-HMX molecular crystals. *J. Phys. D: Appl. Phys.* **2010**, *43*, 035404.

(5) Vial, J.; Picart, D.; Bailly, P.; Delvare, F. Numerical and experimental study of the plasticity of HMX during a reverse edge-on impact test. *Modelling Simul. Mater. Sci. Eng.* **2013**, *21*, 045006.

(6) Luscher, D. J.; Buechler, M. A.; Miller, N. A. Self-consistent modeling of the influence of texture on thermal expansion in polycrystalline TATB. *Modelling Simul. Mater. Sci. Eng.* **2014**, *22*, 075008.

(7) Long, Y.; Chen, J. Theoretical study of phonon density of states, thermodynamic properties and phase transitions for HMX. *Philos. Mag.* **2014**, *94*, 2656−2677.

(8) Barton, N. R.; Winter, N. W.; Reaugh, J. E. Defect evolution and pore collapse in crystalline energetic materials. *Modelling Simul. Mater. Sci. Eng.* **2009**, *17*, 035003.

(9) Cady, H. H.; Ccromer, D. T.; Larson, A. C. Crystal structure of alpha-HMX and a refinement of structure of beta-HMX. *Acta Crystallogr.* **1963**, *16*, 617.

(10) Yoo, C.-S.; Cynn, H. Equation of state, phase transition, decomposition of β-HMX (octahydro-1,3,5,7-tetranitro-1,3,5,7-tetrazocine) at high pressures. *J. Chem. Phys.* **1999**, *111*, 10229−10235.

(11) Choi, C. S.; Boutin, H. P. A study of crystal structure of beta-cyclotetramethylene tetranitramine by neutron diffraction. *Acta Crystallogr., Sect. B: Struct. Sci.* **1970**, *B 26*, 1235.

(12) Stevens, L. L.; Eckhardt, C. J. The elastic constants and related properties of beta-HMX determined by Brillouin scattering. *J. Chem. Phys.* **2005**, *122*, 174701.

(13) Zaug, J. M. Elastic constants of beta-HMX and tantalum, equation of state of supercritical fluids and fluid mixtures and thermal transport determinations. *Proceedings of the 11th International Detonation Symposium*, Snowmass Village, CO, August 31−September 4, 1998; pp 498−509.

(14) Sewell, T. D.; Bedrov, D.; Menikoff, R.; Smith, G. D. Elastic properties of HMX. Shock compression of condensed matter. *Proceedings of 12th International Conference of the American Physical Society Topical Group on Shock Compression of Condensed-Matter*, Atlanta, GA, June 24−29, 2001; pp 399−402.

(15) Zhou, T.-T.; Huang, F.-L. Effects of defects on thermal decomposition of HMX via ReaxFF molecular dynamics simulations. *J. Phys. Chem. B* **2011**, *115*, 278−287.

DOI: 10.1021/acs.jpcb.5b00083
J. Phys. Chem. B XXXX, XXX, XXX−XXX

(16) Zhou, T.; Song, H.; Liu, Y.; Huang, F. Shock initiated thermal and chemical responses of HMX crystal from ReaxFF molecular dynamics simulation. *Phys. Chem. Chem. Phys.* **2014**, *16*, 13914−13931.
(17) Zhang, L.; Zybin, S. V.; Van Duin, A. C. T.; Goddard, W. A., III Modeling high rate impact sensitivity of perfect RDX and HMX crystals by ReaxFF reactive dynamics. *J. Energy Mater.* **2010**, *28*, 92−127.
(18) Conroy, M. W.; Oleynik, I. I.; Zybin, S. V.; White, C. T. First-principles anisotropic constitutive relationships in beta-cyclotetramethylene tetranitramine (beta-HMX). *J. Appl. Phys.* **2008**, *104*, 053506.
(19) Landerville, A. C.; Conroy, M. W.; Budzevich, M. M.; Lin, Y.; White, C. T.; Oleynik, I. I. Equations of state for energetic materials from density functional theory with van der Waals, thermal, and zero-point energy corrections. *Appl. Phys. Lett.* **2010**, *97*, 251908.
(20) Cui, H.-L.; Ji, G.-F.; Chen, X.-R.; Zhang, Q.-M.; Wei, D.-Q.; Zhao, F. Phase Transitions and Mechanical Properties of Octahydro-1,3,5,7-tetranitro-1,3,5,7-tetrazocine in Different Crystal Phases by Molecular Dynamics Simulation. *J. Chem. Eng. Data* **2010**, *55*, 3121−3129.
(21) Peng, Q.; Rahul, A.; Wang, G.; Liu, G. R.; De, S. Structures, mechanical properties, equations of state, and electronic properties of β-HMX under hydrostatic pressures: a DFT-D2 study. *Phys. Chem. Chem. Phys.* **2014**, *16*, 19972−19983.
(22) Warrier, M.; Pahari, P.; Chaturvedi, S. Interatomic potential parameters for molecular dynamics simulations of RDX using a reactive force field: A validation study. *J. Phys. Conf. Ser.* **2012**, *377*, 012100.
(23) Klimes, J.; Michaelides, A. Perspective: Advances and challenges in treating van der Waals dispersion forces in density functional theory. *J. Chem. Phys.* **2012**, *137*, 120901.
(24) Conroy, M. W.; Oleynik, I. I.; Zybin, S. V.; White, C. T. First-principles investigation of anisotropic constitutive relationships in pentaerythritol tetranitrate. *Phys. Rev. B* **2008**, *77*, 094107.
(25) Conroy, M. W.; Oleynik, I. I.; Zybin, S. V.; White, C. T. Density functional theory calculations of solid nitromethane under hydrostatic and uniaxial compressions with empirical van der Waals correction. *J. Phys. Chem. A* **2009**, *113*, 3610−3614.
(26) Grimme, S. Accurate description of van der Waals complexes by density functional theory including empirical corrections. *J. Comput. Chem.* **2004**, *25*, 1463−1473.
(27) Grimme, S. Semiempirical GGA-type density functional constructed with a long-range dispersion correction. *J. Comput. Chem.* **2006**, *27*, 1787−1799.
(28) Grimme, S.; Antony, J.; Ehrlich, S.; Krieg, H. A consistent and accurate ab initio parametrization of density functional dispersion correction (DFT-D) for the 94 elements H-Pu. *J. Chem. Phys.* **2010**, *132*, 154104.
(29) Goerigk, L.; Grimme, S. A thorough benchmark of density functional methods for general main group thermochemistry, kinetics, and noncovalent interactions. *Phys. Chem. Chem. Phys.* **2011**, *13*, 6670−6688.
(30) Grimme, S.; Ehrlich, S.; Goerigk, L. Effect of the damping function in dispersion corrected density functional theory. *J. Comput. Chem.* **2011**, *32*, 1456−1465.
(31) Tkatchenko, A.; Scheffler, M. Accurate molecular van der Waals interactions from ground-state electron density and free-atom reference data. *Phys. Rev. Lett.* **2009**, *102*, 073005.
(32) Tkatchenko, A.; DiStasio, R. A.; Car, R.; Scheffler, M. Accurate and Efficient Method for Many-Body van der Waals Interactions. *Phys. Rev. Lett.* **2012**, *108*, 236402.
(33) Rae, P. J.; Hooks, D. E.; Liu, C. The stress versus strain response of single beta-HMX crystals in quasi-static compression. *Proceedings of the 13th International Detonation Symposium*, Norfolk, VA, July 23−28, 2006; pp 293−300 and pp 399−402.
(34) Kresse, G.; Hafner, J. Ab initio molecular dynamics for liquid metals. *Phys. Rev. B* **1993**, *47*, 558.
(35) Kresse, G.; Furthuller, J. Efficiency of ab-initio total energy calculations for metals and semiconductors using a plane-wave basis set. *Comput. Mater. Sci.* **1996**, *6*, 15.
(36) Hohenberg, P.; Kohn, W. Inhomogeneous electron gas. *Phys. Rev.* **1964**, *136*, B864.
(37) Kohn, W.; Sham, L. J. Self-consistent equations including exchange and correlation effects. *Phys. Rev.* **1965**, *140*, A1133.
(38) Perdew, J. P.; Burke, K.; Ernzerhof, M. Generalized gradient approximation made simple. *Phys. Rev. Lett.* **1996**, *77*, 3865.
(39) Zhang, Y.; Yang, W. Comment on "Generalized gradient approximation made simple. *Phys. Rev. Lett.* **1998**, *80*, 890−890.
(40) Perdew, J. P.; Ruzsinszky, A.; Csonka, G. I.; Vydrov, O. A.; Scuseria, G. E.; Constantin, L. A.; Zhou, X.; Burke, K. Restoring the density-gradient expansion for exchange in solids and surfaces. *Phys. Rev. Lett.* **2008**, *100*, 136406.
(41) Blöchl, P. E. Projector augmented-wave method. *Phys. Rev. B* **1994**, *50*, 17953−17979.
(42) Jones, R. O.; Gunnarsson, O. The density functional formalism, its applications and prospects. *Rev. Mod. Phys.* **1989**, *61*, 689−746.
(43) Timoshenko, S., Goodier, J. N. *Theory of elasticity*, 3rd ed.; McGraw-Hill: New York, 1970.
(44) Bathe, K. J. *Finite Element Procedures*, 2nd ed.; Klaus-Jürgen Bathe: Watertown, MA, 2014.
(45) Herrmann, M.; Engel, W.; Eisenreich, N. Thermal-analysis of the phases of HMX using X-ray diffraction. *Zeitschrift Fur Kristallographie* **1993**, *204*, 121−128.
(46) Deschamps, J. R.; Frisch, M.; Parrish, D. Thermal expansion of HMX. *J. Chem. Crystallogr.* **2011**, *41*, 966−970.
(47) Nye, J. F. *Physical Properties of Crystals*; Oxford Science Publications: Oxford, 1995.
(48) Sun, B.; Winey, J. M.; Gupta, Y. M.; Hooks, D. E. Determination of second-order elastic constants of cyclotetramethylene tetranitramine (β-HMX) using impulsive stimulated thermal scattering. *J. Appl. Phys.* **2009**, *106*, 053505.
(49) Sewell, T. D.; Menikoff, R.; Bedrov, D.; Smith, G. D. A molecular dynamics simulation study of elastic properties of HMX. *J. Chem. Phys.* **2003**, *119*, 7417−7426.
(50) Greaves, G. N.; Greer, A. L.; Lakes, R. S.; Rouxel, T. Poisson's ratio and modern materials. *Nat. Mater.* **2011**, *10*, 823−837.
(51) Pettifor, D. G. Theoretical predictions of structure and related properties of intermetallics. *Mater. Sci. Technol.* **1992**, *8*, 345−349.
(52) Dlott, D. D.; Fayer, M. D. Shocked molecular-solids - vibrational up pumping, defect hot spot formation, and the onset of chemistry. *J. Chem. Phys.* **1990**, *92*, 3798−3812.

DOI: 10.1021/acs.jpcb.5b00083
J. Phys. Chem. B XXXX, XXX, XXX−XXX